Surface modes of liquid ^{4}He

K. A. Gernoth and J. W. Clark
McDonnell Center for the Space Sciences and Department of Physics, Washington University, St. Louis, Missouri 63130

G. Senger and M. L. Ristig
Institut für Theoretische Physik, Universität zu Köln, D-50937 Köln, Germany
(Received 28 February 1994)

This method of correlated basis functions is applied at the variational level to give an optimized description, at zero temperature, of the structure and elementary excitations of liquid ^{4}He in the geometry of a half-space. A trial ground-state wave function of Hartree-Jastrow form is assumed, and the Feynman ansatz is adapted to construct trial elementary excitations based on this variational ground state. Functional variation of the energy expectation value with respect to ground and excited trial states leads, in conjunction with the Bogoliubov-Born-Green-Kirkwood-Yvon relations and the hypernetted-chain (HNC) equations, to coupled Euler-Lagrange equations consisting of (i) a modified Hartree equation, (ii) a paired-phonon equation, and (iii) a renormalized Bogoliubov eigenvalue equation. These relations and equations provide for simultaneous optimal determination of (i) the density profile, the chemical potential, and the Hartree inhomogeneity factor, (ii) the anisotropic two-body pseudopotential and two-body spatial distribution function, and (iii) the wave functions and energies of the Feynman excitations as functions of the momentum parallel to the surface plane. In the numerical calculation reported, the bulk liquid density is taken equal to the experimental value at saturation. Since the corresponding Jastrow variational treatment of the bulk liquid does not produce a self-bound system at this density, an external potential is introduced to stabilize the surface, its strength being adjusted so that the calculated chemical potential matches the experimental saturation value. The calculation yields dispersion relations for two distinct branches of bound surface states, extending from the continuum of liquid states at small wave numbers to the continuum of liquid states close to the wave number characteristic of a bulk roton. The two branches are distinguished by the number of nodes (zero or one) of the corresponding wave functions in the surface region. At small wave numbers, the wave functions of the lowest-lying surface states penetrate exponentially into the bulk liquid to a characteristic depth proportional to wavelength. These modes are associated with surface phonons and capillary waves, being driven by the external potential (renormalized by correlation effects due to the strong internal forces) and by the surface tension. The spectrum of surface excitations of the first branch follows the hydrodynamic dispersion relation in the range of wave numbers $0 \leq q \leq 0.5$ Å^{-1}. Employing a specialized version of the renormalized Bogoliubov equation, analytic expressions are derived that permit evaluation of the speed of surface sound and the surface-tension coefficient in terms of quantities generated by the microscopic calculation. In the opposite regime of large wave numbers corresponding to the atomic scale, $q \geq 1$ Å^{-1}, the wave functions of the first branch are centered at a local density approaching that of the bulk liquid. The dispersion curves of both branches appear to terminate by merging with the bulk excitation curve near the roton minimum, in conformity with the interpretation of the bound surface states in this wave-number range as trapped rotons.

I. INTRODUCTION

The propagation of surface and interface waves in liquid helium continues to be of fundamental experimental and theoretical interest. Helium surfaces, interfaces, and films present unique opportunities for studying the effects of large quantum fluctuations and of strong correlations in condensed matter. The associated elementary excitations can be driven by external forces such as gravity or van der Waals forces exerted on the helium liquid by the surrounding walls or by a supporting substrate. They can also be driven by internal forces via the surface or interfacial tension of the self-bound system.[1] Experimental information on the propagation of surface excitations is best at small wave numbers where the dispersion of gravitational waves, surface sound, and capillary waves is theoretically described by quantized hydrodynamic models.[1,2] References 3 and 4 report some experimental results on these modes and give an analysis within Atkins' description.[1]

However, such a description is not suitable for the elementary excitations at large energies and at atomic wavelengths, which have been recently explored in neutron-scattering experiments.[5,6] To carry out a proper theoretical analysis of surface or interface excitations at high momenta parallel to the surface or interface plane, one must go beyond the standard hydrodynamic model. Ideally, one should pursue systematic improvements within an *ab initio* approach. Important early steps in this direction have been made by Chang and Cohen,[7] Edwards and Saam,[2] Ji and Wortis,[8] and, more recently, by Pitaevskii and Stringari.[9]

Restricting attention to surface phenomena of liquid ^{4}He at *zero* temperature, we may exploit the theory of inhomogeneous quantum fluids that has been developed within the method of correlated basis functions[10–13] by Krotscheck and co-workers.[14–16] This theory, which expands upon earlier work of Saarela, Pietiläinen, and Kallio,[17] is an explicit realization of the correlated basis functions (CBF) approach at the variational level, entailing determination of the optimal correlated Hartree-Jastrow ground state and the optimal wave functions and energies of elementary excitations in Feynman approximation.[18] The subsequent inclusion of backflow effects[11,19] does not pose any difficulties of principle. Since, as in Refs. 20–24, we still ignore backflow effects, the theoretical excitation energies calculated at large wave numbers q are substantially higher than the experimental results. We stress that CBF theory[11–13,25] affords systematic means of incorporating backflow correlations.

Within this restricted context, we are at liberty to study theoretically both the bulk and surface modes in liquid ^{4}He at arbitrary wave number q. Moreover, we may simultaneously improve upon the hydrodynamic description of the long-wavelength surface modes since the optimization process yields incisive formal results for the speed of surface sound and the phase velocity of capillary waves that permit quantitative evaluation of these physical quantities.

During the last few years the CBF theory of inhomogeneous Bose fluids has been primarily applied to thin ^{4}He films with or without a supporting substrate and notably to the elementary excitations of these systems.[20–23] This emphasis is due to the special interest in the physics of helium films,[5,6] but also in part to the possibility of reducing the complexity of the numerical task relative to that of the free-surface problem.

Here, we shall concentrate on a microscopic CBF treatment of the bound surface modes of liquid ^{4}He at zero temperature and at experimental saturation density, considering a planar surface profile in the geometry of an infinitely extended half-space. The density profile is shaped by an appropriately chosen external single-particle potential. This work continues along the lines of a recent analysis of the excitation spectrum of the vapor-liquid ^{4}He interface[24] and proceeds toward a consistent optimization of the excitation energies within the specialization to zero temperature. We arrive at improved theoretical descriptions of the elementary surface excitations over the pertinent range in the momentum $\hbar\mathbf{q}$ parallel to the planar surface. The improvement at small wave numbers is of vital importance.

The *ab initio* study of liquid ^{4}He with a planar surface is based on the many-body Hamiltonian

$$H_N = T + V + U \ , \tag{1}$$

which underlies the microscopic behavior of N ^{4}He atoms (with $N \to \infty$ in the thermodynamic limit). The surface is parallel to the (x,y) plane and, consequently, the local density ρ of the liquid depends only on the coordinate z, i.e., $\rho = \rho(z)$. As $z \to -\infty$ the properties of the system approach those of the bulk liquid, whereas the density $\rho(z)$ falls off to zero as $z \to \infty$. The kinetic operator T is represented by $-(\hbar^2/2m)\sum_{i=1}^{N}\nabla_i^2$ and the internal potential V by a sum of pair potentials $v(ij)$ of purely radial form $v(r_{ij})$, where $r_{ij} = |\mathbf{r}_{ij}|$ is the relative distance between ^{4}He atoms i and j. The potential function $v(r)$ is assumed to be of Lennard-Jones (6,12) shape with the standard ^{4}He parameters $\varepsilon_{LJ} = 10.22$ K and $\sigma_{LJ} = 2.556$ Å, respectively. The external potential U, taken as a sum of single-particle potentials $U_{\text{ext}}(z_i)$, is introduced to balance the pressure inside the liquid.

It is well known that the theoretical value of the chemical potential of homogeneous bulk liquid ^{4}He at (experimental) saturation density $\rho_L = 0.0218$ Å^{-3}, calculated on the Jastrow variational level of CBF theory, is positive—and thus fails to reproduce the experimental value $\mu = -7.17$ K. Accordingly, the Hartree equation delineating the one-particle structure [Eq. (9) of Sec. II] does not possess a self-bound solution at that density. To circumvent this problem, we apply an external single-particle potential of the form

$$U_{\text{ext}}(z) = \frac{U_0}{1 + \exp[\alpha(z - z_W)]} \ , \tag{2}$$

which varies strongly with z in the surface region and becomes constant in the homogeneous density regime. The strength parameter U_0 is adjusted so that the calculated chemical potential μ equals the experimental saturation value. The choice of 11.4 Å made for z_W is arbitrary and localizes the Gibbs dividing surface at $z_G = 12.8$ Å, while α is specified by

$$\alpha = \{-2m\,[\mu - V_H(L_2) - U_{\text{ext}}(L_2)]/\hbar^2\}^{1/2} \ , \tag{3}$$

where L_2 marks the "right" boundary of the finite box $[-L_1 \le z \le L_2]$ in which the numerical calculation is performed. In addition to its role in pressure balance, the external potential expedites the convergence of the paired-phonon analysis (PPA) iteration scheme, particularly in the low-density tail where the local particle-number density is smaller than $0.1\rho_L$.

CBF theory furnishes Euler-Lagrange equations for determining the optimal density profile $\rho(z)$, the optimal spatial distribution function $g(\mathbf{r}_1,\mathbf{r}_2)$, and the optimal wave functions and energies that describe the existing volume and surface modes of the ^{4}He system. These equations consist of (i) a renormalized Hartree equation[14,17] for the square root of the density profile, $\sqrt{\rho(z)}$, (ii) a paired-phonon (PPA) equation[14] for the spatial distribution function $g(\mathbf{r}_1,\mathbf{r}_2)$ of the ^{4}He liquid ground state, which contains the excitations virtually, and (iii) a renormalized Bogoliubov equation or, equivalently, a Feynman equation for the wave functions and energies of the elementary excitations.[15,16] These equations are solved numerically with sufficient accuracy by means of efficient iteration procedures.

In accordance with the symmetry of the system, an elementary excitation carries a momentum $\hbar\mathbf{q} \equiv \hbar(q_x,q_y)$ parallel to the surface plane. The associated states may belong to differing classes of continuum states or to differing branches of bound surface states.[24] The latter states have energies that are below the energy spectrum of the continuum states at fixed wave number $q \equiv |\mathbf{q}|$.

The ^{4}He system studied in this work possesses two distinct branches of bound surface states, extending in the energy-momentum diagram from the continuum of liquid states at small wave numbers $q \leq 0.5$ Å^{-1} to the continuum of liquid states close to the wave number $q_R \simeq 1.9$ Å^{-1} of a bulk roton.

In our numerical explorations we are especially interested in the nature of the lowest branch of bound surface states. These states are localized and centered within the inhomogeneous surface layer, having no nodes therein. At long wavelengths ($0 \leq q \leq 0.8$ Å^{-1}) the wave functions penetrate exponentially into the bulk liquid, the depth of penetration being measured by the inverse wave number q^{-1}. The corresponding excitation energies follow the dispersion law of surface phonons and of capillary waves. Exploiting the properties of the renormalized Bogoliubov equation, we may extract explicit formal expressions for the phase velocity of long-wavelength surface waves that admit quantitative evaluation. At atomic wavelengths (1 Å$^{-1} \leq q \leq q_R$) the new results for the optimized wave functions and energies of the lowest branch of bound states essentially confirm our earlier findings, reported in Ref. 24. The associated wave functions are localized in the surface layer, in general with a small width, their corresponding energies approaching the bulk roton energy regime at large wave numbers $q \simeq q_R$. These states are interpreted as trapped rotons.

Section II collects the basic Euler-Lagrange equations needed for numerical determination of the optimized ground and excited states. Numerical results on the bound surface wave functions are displayed and described in Sec. III. Surface phonons, capillary waves, and trapped rotons are treated in Sec. IV and Sec. V. The paper concludes with comments on possible improvements, applications, and future prospects (Sec. VI).

II. CBF FORMALISM AND PROCEDURES

The variational-CBF theory of liquid ^{4}He with a planar surface begins by adopting a correlated ground-state wave function of Hartree-Jastrow form,

$$\Psi_N(\mathbf{R}) = \exp\left[\frac{1}{2}\sum_{i=1}^{N} t(z_i) + \frac{1}{2}\sum_{i<j}^{N} u(\eta_{ij},z_i,z_j)\right] . \tag{4}$$

The single-particle function $t(z_i)$ depends on the distance z_i of atom i from the (x,y) plane, which is taken parallel to the ^{4}He surface. It is sometimes convenient—but not necessary—to measure this distance from the Gibbs dividing surface, positioning the origin of the r-space coordinate system accordingly. The spatial correlations of the strongly interacting ^{4}He atoms (i and j) are described by the pseudopotential $u(\eta_{ij},z_i,z_j)$, which is a function of the distances z_i and z_j and of the projection $\eta_{ij} = [(x_i - x_j)^2 + (y_i - y_j)^2]^{1/2}$ of the relative vector $\mathbf{r}_{ij} = \mathbf{r}_i - \mathbf{r}_j$ onto the (x,y) plane. The correlated ground state represented by Eq. (4) contains *virtually* the elementary excitations of the many-body system.

Based on the Hamiltonian (1) and ansatz (4), variational-CBF theory provides a practical framework for evaluating the functions $t(z_1)$ and $u(\eta_{12},z_1,z_2)$ and, simultaneously, the local density $\rho(z_1)$ (the density profile), the spatial distribution function $g(\eta_{12},z_1,z_2)$, and the wave functions of the elementary excitations (or the density-fluctuation operators) and their energies. The formal relation between the functions t,u and ρ,g is given by the Bogoliubov-Born-Green-Kirkwood-Yvon equation[22] and the hypernetted-chain (HNC) equations.[14,17,26] The latter set of equations rests on the decomposition of the function g into nodal (N) and non-nodal (X) portions. In the present case the HNC equations read[17,24,26] (with $\eta \equiv \eta_{12}$)

$$g(\eta,z_1,z_2) = 1 + X(\eta,z_1,z_2) + N(\eta,z_1,z_2) , \tag{5}$$

$$X(\eta,z_1,z_2) = \exp\{u(\eta,z_1,z_2) + N(\eta,z_1,z_2) + E(\eta,z_1,z_2)\} - N(\eta,z_1,z_2) - 1 , \tag{6}$$

$$N(q,z_1,z_2) = \int_{-\infty}^{\infty} \rho(z_3)\{X(q,z_1,z_3) + N(q,z_1,z_3)\} \times X(q,z_3,z_2)\,dz_3 . \tag{7}$$

The hypernet equation (6) involves a function $E(\eta,z_1,z_2)$ that embodies the elementary or bridge contributions.[25] It is set zero in the HNC/0 approximation adopted in this study. The functions $X(\eta,z_1,z_2)$ and $N(\eta,z_1,z_2)$ may be viewed as coordinate-space matrix elements defining operators X and N, respectively. The chain equation (7) is formulated in terms of the Hankel transforms of the quantities X and N. The Hankel transform $\mathcal{H}[f_\eta]$ of a function $f(\eta,z_1,z_2) \equiv f_\eta(z_1,z_2)$ is

$$f(q,z_1,z_2) \equiv f_q(z_1,z_2) = 2\pi \int_0^{\infty} f(\eta,z_1,z_2) J_0(q\eta)\eta\, d\eta , \tag{8}$$

wherein J_0 is the zeroth-order Bessel function of the first kind.[27]

The reader may consult Refs. 14–17 and 20–23 for detailed formulations of the variational-CBF approach, including derivations of the Euler-Lagrange equations for the density profile $\rho(z)$, the spatial distribution function $g(\eta,z_1,z_2)$, and the optimal Feynman wave functions and their energy eigenvalues.

The optimal density profile is characterized by its square root $\sqrt{\rho(z)}$, which is determined by a renormalized Hartree equation.[14,17] In Dirac notation the latter reads

$$\{T_z + U_{\text{ext}} + V_H\}|0\rangle = \mu|0\rangle , \tag{9}$$

where $|0\rangle$ is the one-body ground state in the mean field, an eigenvector with vanishing momentum ($\hbar\mathbf{q} = 0$). The amplitude $\langle z|0\rangle > 0$ gives the square root of the density profile, $\langle z|0\rangle = \sqrt{\rho(z)}$. The state $|0\rangle$ is generated by the single-particle operator T_z, represented by $-(\hbar^2/2m)d^2/dz^2$, the external potential (2), and the Hartree mean-field potential V_H, which is explicitly defined in Eq. (19). The energy μ is the chemical potential of the system.

The Euler-Lagrange equation for the optimal spatial distribution function $g(\eta,z_1,z_2)$ may be written in the form of a paired-phonon equation[11] for the correlation operator $\tilde{X}$ defined by the matrix elements

$\sqrt{\rho(\mathbf{r}_1)\rho(\mathbf{r}_2)}X(\mathbf{r}_1,\mathbf{r}_2)$ in coordinate space. In Dirac notation we have[14,15]

$$-\{H\tilde{X}+\tilde{X}H\}+\tilde{X}H\tilde{X}=2\tilde{V}_{\rm ph} \ . \tag{10}$$

For a homogeneous boson fluid, this prescription specializes to the original paired-phonon equation introduced by Feenberg and Campbell.[11,13] The name derives from the fact that the equation is obtained within a paired-phonon analysis (PPA) of the many-body Hamiltonian eigenvalue problem of the uniform Bose system, which is carried out in a wave function space generated by product functions compounded from (a) a starting trial ground-state factor of Jastrow type, (b) paired-phonon factors $\rho_{\mathbf{k}}\rho_{-\mathbf{k}}$ taken to all powers (where $\rho_{\mathbf{k}}$ is a phonon creation operator), and (c) multiple-phonon factors $\rho_{\mathbf{k}}\cdots\rho_{\mathbf{k}'}$ to all powers, with neglect of processes in which phonons scatter, split, or coalesce. Campbell and Feenberg established that the optimal ground-state trial function constructed within this space is still a symmetrical product of two-body factors, i.e., still of Jastrow form, and with the PPA equation as the key ingredient, they formulated a consistent scheme for practical determination of the optimal pair correlations.

The solution $\tilde{X}$ of Eq. (10) is driven by a renormalized particle-hole operator $\tilde{V}_{\rm ph}$ with elements $\sqrt{\rho(\mathbf{r}_1)\rho(\mathbf{r}_2)}V_{\rm ph}(\mathbf{r}_1,\mathbf{r}_2)$. This operator is the appropriate generalization of the bare particle-hole interaction that appears in the familiar result for the static form factor $S(k)$ of a quantum fluid in the random-phase approximation.[14] Explicit expressions for the matrix elements of the particle-hole interaction V_{ph} in coordinate-space representation are given in Eq. (21). The Hankel transform of the coordinate-space representation of the one-particle effective kinetic operator H appearing in Eq. (10) may be cast into the form $H(q)=H_0+\varepsilon_0(q)$, where $\varepsilon_0(q)=\hbar^2q^2/2m$ is the energy of a free ^{4}He atom with momentum $\hbar\mathbf{q}$ (parallel to the surface) and

$$H_0=-\frac{\hbar^2}{2m}\frac{1}{\sqrt{\rho(z)}}\frac{\partial}{\partial z}\rho(z)\frac{\partial}{\partial z}\frac{1}{\sqrt{\rho(z)}} \ . \tag{11}$$

A renormalized Bogoliubov equation[15,16] determines the optimal Feynman eigenstates and energies corresponding to the elementary excitations of the discrete and continuous spectra. In Dirac notation we may rewrite this equation as

$$\{H^2+2\tilde{V}_{\rm ph}H\}|\psi_{\kappa,\mathbf{q}}\rangle=\varepsilon_\kappa^2(q)|\psi_{\kappa,\mathbf{q}}\rangle \ . \tag{12}$$

The continuum eigenstates are represented—deep inside the bulk liquid—by plane waves $\langle\mathbf{r}|\psi_{\kappa,\mathbf{q}}\rangle=\exp(i\mathbf{k}\cdot\mathbf{r})$ (or, equivalently, by standing plane waves[24]) with wave vectors $\mathbf{k}=\mathbf{q}+\mathbf{k}_\perp$. In this case, the continuous quantum number κ becomes the transverse momentum $\mathbf{k}_\perp$ orthogonal to the (x,y) surface plane. A comprehensive discussion of the various kinds of continuum states has been given in Ref. 24. Here we will focus on the bound surface states. These are specified by a given parallel momentum $\hbar\mathbf{q}$ and an integral quantum number κ, with $\kappa-1$ equal to the number of nodes possessed by the bound state wave function in the inhomogeneous surface layer. We follow the notation of Ref. 24 in characterizing and classifying the various excited states.

Equivalently, Eq. (12) may be expressed in the more familiar form of a Feynman eigenvalue equation[22,24]

$$\{H-\tilde{X}H\}|\psi_{\kappa,\mathbf{q}}\rangle=\varepsilon_\kappa(q)|\psi_{\kappa,\mathbf{q}}\rangle \ . \tag{13}$$

The solutions of Eq. (13) yield the optimal wave functions $\langle\mathbf{r}|\psi_{\kappa,\mathbf{q}}\rangle$ if the correlation operator fulfills the paired-phonon equation (10) (see Refs. 16 and 22). In the cases of immediate interest, all wave functions contain a plane-wave factor carrying the parallel momentum $\hbar\mathbf{q}$, i.e., we have

$$\langle\mathbf{r}|\psi_{\kappa,\mathbf{q}}\rangle=\exp[i(q_xx+q_yy)]\psi_\kappa(z,q) \ .$$

Therefore the discussion of bound surface excitations (which will engross Secs. III–V) centers on the nontrivial factor $\psi_\kappa(z,q)$.

In solving the HNC equations (5)–(7), the technique commonly applied to the homogeneous phase[11,13] is followed as closely as possible, especially with regard to separate treatment of the short- and long-range portions of the various two-body quantities. Thus we assert the decomposition

$$u=u_{\rm SV}+\delta u \ , \tag{14}$$

where the short-range part is assumed to be of Schiff-Verlet form

$$u_{\rm SV}(\eta,z_1,z_2)=-\left[\frac{b_0+b_1\sqrt{\rho(z_1)\rho(z_2)}}{\sqrt{\eta^2+(z_1-z_2)^2}}\right]^5 \tag{15}$$

with the parameters $b_0=2.8$ Å and $b_1=9.98$ Å^4 taken from Ref. 21. The term δu represents the long-range part that remains to be calculated. Analogous decompositions are made for the nodal function N and the direct correlation function X,

$$N=N_{\rm sr}-\delta u \ , \tag{16a}$$

$$X=X_{\rm sr}+\delta u \ . \tag{16b}$$

The quantities $N_{\rm sr}$ and $X_{\rm sr}$ are of short range, in contrast to the correction δu to the Jastrow pseudopotential. In terms of these short-range functions, the spatial distribution function (5) may be given the equivalent expression $g=1+X_{\rm sr}+N_{\rm sr}$ and the hypernet equation (6) in HNC/0 approximation appears as

$$X_{\rm sr}=\exp(u_{\rm SV}+N_{\rm sr})-N_{\rm sr}-1 \ . \tag{17}$$

The general computational scheme adopted to solve the set of coupled HNC and Euler-Lagrange equations begins with iterative solution of the renormalized Hartree equation (9), using as inputs the Schiff-Verlet ansatz, i.e., $\delta u\equiv0$, and a parametrized density profile ρ of the form employed in Ref. 30. It is of course necessary to solve the HNC equations every time the actual density profile is altered. This procedure generates a function $\rho(z)$ that is optimal for the short-range Schiff-Verlet pseudopotential (15). With the resulting $\rho(z)$ and $u_{\rm SV}(\eta,z_1,z_2)$ as inputs, we solve the PPA equation (10) to obtain an improved two-body pseudopotential $u=u_{SV}+\delta u$. Thereupon, the

HNC equations are solved once more before finally updating the density $\rho(z)$ via Eq. (9), keeping the long-range function δu fixed. At this point the first full PPA cycle has been completed. In our present study, eight PPA cycles are required to achieve satisfactory convergence of the entire procedure. After eight PPA cycles, the values for the (free-system) chemical potential $\lim_{z\to-\infty} V_H(z)$ and the surface tension, as well as the values for the surface and bulk excitation energies, are stable within $\approx 2\%$. To the same accuracy, we reproduce the optimized excitation energies of the homogeneous bulk liquid at any of the wave numbers considered. Specifically, we reproduce the precisely calculated bulk excitation energies within $\approx 2\%$ accuracy. Furthermore, the speed of ordinary sound obtained for the inhomogeneous system is in reasonable agreement with the corresponding result for the homogeneous problem (see Sec. IV).

At prescribed bulk density ρ_L and chemical potential μ, the renormalized Hartree equation (9) is solved by means of a Newton-Raphson procedure[17] with input function[30]

$$\rho_{ST}(z)=\rho_L(1+\exp[(z-z_0)/a])^{-\alpha} \tag{18}$$

taking parameters $a=1.5$ Å, and $z_0=15.5$ Å. The Hartree mean-field potential V_H reads explicitly

$$V_H(z_1)=2\pi\int_{-\infty}^{\infty}\rho(z_2)\int_0^{\infty}F_H(\eta,z_1,z_2)\eta\,d\eta\,dz_2-2\pi\frac{\hbar^2}{8m}\int_{-\infty}^{\infty}\rho(z_2)\int_0^{\infty}(\partial_{z_2}N)(\partial_{z_2}X)(\eta,z_1,z_2)\eta\,d\eta\,dz_2$$
$$-2\pi\frac{\hbar^2}{8m}\int_{-\infty}^{\infty}\rho(z_2)\int_0^{\infty}(\partial_{\eta}N)(\partial_{\eta}X)(\eta,z_1,z_2)\eta\,d\eta\,dz_2\ , \tag{19}$$

wherein $\partial_{z_2}N$ (for example) denotes the partial derivative of the function N with respect to the variable z_2, the other arguments of N being held fixed. The function F_H appearing in the integrand is defined as

$$F_H(\eta,z_1,z_2)=[gv](\eta,z_1,z_2)+\frac{\hbar^2}{8m}[g\{2[\partial_\eta u_{SV}+\partial_\eta N_{sr}]^2+[\partial_{z_1}u_{SV}+\partial_{z_1}N_{sr}]^2+[\partial_{z_2}u_{SV}+\partial_{z_2}N_{sr}]^2\}](\eta,z_1,z_2)$$
$$-\frac{\hbar^2}{8m}[g(\partial_{z_1}u_{SV}+\partial_{z_1}N_{sr})(\partial_{z_1}N)+g(\partial_{z_2}u_{SV}+\partial_{z_2}N_{sr})(\partial_{z_2}N)](\eta,z_1,z_2)$$
$$-\frac{\hbar^2}{4m}[g(\partial_\eta u_{SV}+\partial_\eta N_{sr})(\partial_\eta N)](\eta,z_1,z_2)\ . \tag{20}$$

The PPA equation (10) contains a particle-hole operator determined by

$$V_{ph}(\eta,z_1,z_2)=[gv](\eta,z_1,z_2)+\frac{\hbar^2}{8m}[g\{2[\partial_\eta u_{SV}+\partial_\eta N_{sr}]^2+[\partial_{z_1}u_{SV}+\partial_{z_1}N_{sr}]^2+[\partial_{z_2}u_{SV}+\partial_{z_2}N_{sr}]^2\}](\eta,z_1,z_2)$$
$$-\tfrac{1}{2}[(g-1)\{\mathcal{H}^{-1}[R_q]+[\hat{D}(z_1)+\hat{D}(z_2)]N\}](\eta,z_1,z_2)\ . \tag{21}$$

In the second line, the inverse $\mathcal{H}^{-1}$ of the Hankel transform operates on

$$R(q,z_1,z_2)\equiv R_q(z_1,z_2)=2\varepsilon_0(q)N(q,z_1,z_2)+C(q,z_1,z_2)\ . \tag{22}$$

The function C is defined by

$$C(q,z_1,z_2)=\frac{\hbar^2}{2m}\int_{-\infty}^{\infty}\rho(z_3)[\partial_{z_3}X_q(z_1,z_3)][\partial_{z_3}X_q(z_3,z_2)]dz_3+\varepsilon_0(q)[X_q\circ X_q](z_1,z_2)\ , \tag{23}$$

where the last term involves the convolution operation

$$[f\circ h](z_1,z_2)=\int_{-\infty}^{\infty}\rho(z_3)f(z_1,z_3)h(z_3,z_2)dz_3\ . \tag{24}$$

Equation (21) involves the operator

$$\hat{D}(z)=-\frac{\hbar^2}{2m}\frac{\partial^2}{\partial z^2}-\frac{\hbar^2}{2m}\mathcal{G}(z)\frac{\partial}{\partial z}\ , \tag{25}$$

with $\mathcal{G}(z)=(\ln[\rho(z)])'$.

For the purposes of numerical analysis, we make use of the HNC equations (7) and (17) and the decompositions (14) and (16) to recast the PPA condition (10) into the form

$$[2\varepsilon_0(q)+\hat{D}(z_1)+\hat{D}(z_2)]\delta u(q,z_1,z_2)=-2\delta V(q,z_1,z_2)+\delta C(q,z_1,z_2)\ . \tag{26}$$

In this guise the PPA condition becomes an equation for the optimal correction $\delta u(q,z_1,z_2)$ to the Schiff-Verlet pseudopotential. It is this equation which, at any wave number q, is solved numerically for the quantity $\delta u(q,z_1,z_2)$ by means of an iterative relaxation procedure, in order to obtain the optimal pseudopotential u via the decomposition (14). The

quantity δV appearing in Eq. (26) is given by

$$\delta V(q,z_1,z_2)=\mathcal{H}[\delta V_1](q,z_1,z_2)-\tfrac{1}{2}C_{\rm sr}(q,z_1,z_2)\ , \tag{27}$$

where $C_{\rm sr}$ is the short-range portion of Eq. (23) (obtained by taking $X_{\rm sr}$ instead of X). The function δV_1 is constructed as

$$\begin{aligned}\delta V_1(\eta,z_1,z_2)=&[gv](\eta,z_1,z_2)-\frac{\hbar^2}{8m}[g\{2[\partial_\eta u_{\rm SV}+\partial_\eta N_{\rm sr}]^2+[\partial_{z_1}u_{\rm SV}+\partial_{z_1}N_{\rm sr}]^2+[\partial_{z_2}u_{\rm SV}+\partial_{z_2}N_{\rm sr}]^2\}](\eta,z_1,z_2)\\&+\left[g\left\{-\frac{\hbar^2}{2m}[\eta^{-1}\partial_\eta+\partial_\eta^2]u_{\rm SV}+\tfrac{1}{2}[\hat D(z_1)+\hat D(z_2)]u_{\rm SV}\right\}\right](\eta,z_1,z_2)\\&+\tfrac{1}{2}[(g-1)\{\mathcal{H}^{-1}[G_q]+[\hat D(z_1)+\hat D(z_2)]\delta u\}](\eta,z_1,z_2)\ ,\end{aligned} \tag{28}$$

where

$$G_q\equiv G(q,z_1,z_2)=2\varepsilon_0(q)\delta u(q,z_1,z_2)-C(q,z_1,z_2)\ , \tag{29}$$

with C defined in Eq. (23). In addition to the contribution $-2\delta V$, a second term δC enters Eq. (26). Introducing the abbreviation

$$\begin{aligned}[f*h](z_1,z_2)=&\varepsilon_0(q)[f\circ h](z_1,z_2)\\&+\frac{\hbar^2}{2m}[\partial_{z_3}f(z_1,z_3)\circ\partial_{z_3}h(z_3,z_2)](z_1,z_2)\ ,\end{aligned} \tag{30}$$

the quantity δC may be written as

$$\begin{aligned}\delta C(q,z_1,z_2)=&([\delta u_q*X_{{\rm sr},q}]+[X_{{\rm sr},q}*\delta u_q]\\&+[\delta u_q*\delta u_q])(z_1,z_2)\ .\end{aligned} \tag{31}$$

To calculate the excitation energies and eigenfunctions of the Bogoliubov equation (12), we essentially follow Ref. 24, imposing the boundary conditions

$$\frac{d}{dz}\psi_\kappa(z,q)=0 \tag{32}$$

and

$$\frac{d}{dz}\psi_\kappa(z,q)=\alpha\psi_\kappa(z,q) \tag{33}$$

at the liquid and low-density sides, respectively. The numerical results for the energies and wave functions will be discussed in the following sections.

Figures 1 and 2 show some of our results for the optimal density profile $\rho(z)$ and optimal spatial distribution function $g(\eta,z_1,z_2)$. The Euler-Lagrange equations are solved at the experimental saturation density $\rho_L=0.0218$ Å^{-3}, employing the external potential (2) with the choices of α and z_W indicated previously and the strength U_0 chosen such that the chemical potential $\mu=U_0+\lim_{z\to-\infty}V_H(z)$ of the system matches the experimental value at saturation, -7.17 K. Figure 1 displays the numerical results for the local density $\rho(z)$, the external potential $U_{\rm ext}(z)$, and the total one-body potential $V_H(z)+U_{\rm ext}(z)$. The density profile (solid curve) approaches its asymptotic value ρ_L as $z\to-\infty$ and vanishes exponentially as $z\to+\infty$. The surface has a 90–10% width of approximately 4.9 Å. Within the liquid, the total one-body potential $V_H(z)+U_{\rm ext}(z)$ (dot-dashed curve) approaches the experimental binding energy per particle, i.e., the chemical potential at saturation, by construction. This function has a shallow minimum in the center of the surface region and vanishes as $z\to+\infty$.

Selected results for the optimal spatial distribution function $g(\eta,z_1,z_2)$ are presented in Fig. 2. We display numerical data for the case that atom 2 is localized at $z_2=-L_1$ and atom 1 is displaced in either the η or the z coordinate, where L_1 denotes the "left" boundary of the box $[-L_1\le z\le L_2]$ employed for our numerical calculations. Since these data points probe the correlations deep inside the bulk region, we expect the results for $g(\eta,z_1=-L_1,z_2=-L_1)$ and for $g(\eta=0,z_1,z_2=-L_1)$, as functions of $r_{12}=\eta$ and $r_{12}=z_1-z_2$, respectively, to agree well with each other and with the results for the radial distribution function $g(r_{12})$ calculated within variational-CBF theory for bulk liquid ^{4}He at density ρ_L. Inspecting the results for the first of these functions (open dots), for the second (full dots), and for the radial distri-

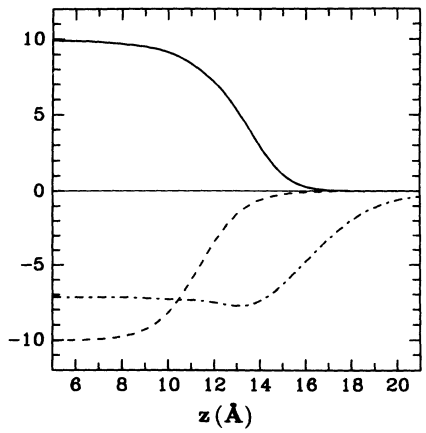

FIG. 1. Optimal density profile $\rho(z)$ (full curve), chosen external potential $U_{\rm ext}(z)$ (long-dashed curve), and the superposition $U_{\rm ext}(z)+V_H(z)$ (dot-dashed curve) entering the Hartree equation (9), as functions of position z (in units of Kelvin). The Gibbs surface of the inhomogeneous system is located at $z_G=12.8$ Å. On the scale employed, the bulk density $\rho_L=0.0218$ Å^{-3} corresponds to 10 K.

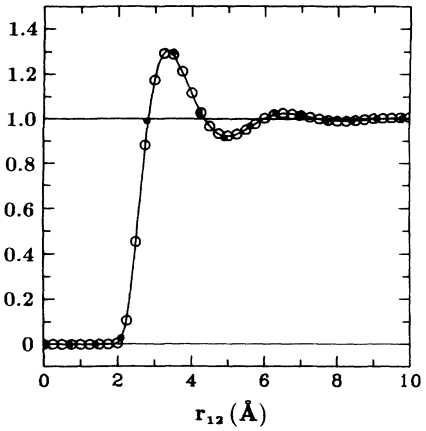

FIG. 2. Optimal spatial distribution function $g(\mathbf{r}_1,\mathbf{r}_2)$ versus two-particle distance $r_{12}=|\mathbf{r}_1-\mathbf{r}_2|$. Shown are the particular cases (i) $z_1=z_2=-L_1, r_{12}=\eta$ (open dots) and (ii) $\eta=0, r_{12}=|z_1-z_2|$ with $z_2=-L_1$ fixed (full dots). The results are compared with the radial distribution function $g(r_{12})$ of bulk liquid ^{4}He at saturation density ρ_L (solid curve). As expected, the three sets of results are in excellent agreement, since they describe correlations deep inside the liquid.

bution of the isotropic bulk liquid (full curve), this expectation is seen to be confirmed with excellent accuracy. The indicated agreement is in accord with the findings of Ref. 31 on the spatial distribution function in the center of a thick planar ^{4}He film.

III. BOUND SURFACE MODES

To provide a basis for quantitative considerations of the nature of the elementary excitations of liquid ^{4}He with a planar surface, we have solved, simultaneously, the Hartree equation, the paired-phonon equation, and the Bogoliubov equation, in conjunction with the HNC equations in HNC/0 approximation. The input external potential (2) is chosen such that the chemical potential μ reproduces the experimental binding energy per atom of 7.17 K at saturation density $\rho_L=0.0218$ Å^{-3}. Figure 1 depicts the shape of this potential together with the resulting optimal total one-particle potential $U_{\rm ext}(z)+V_H(z)$ entering the Hartree equation. The corresponding optimal ^{4}He density profile $\rho(z)$ is drawn in the same figure. It is a smooth function of the distance z, monotonically approaching the bulk density ρ_L in the homogeneous liquid regime. In the region of *very* low densities, the profile vanishes exponentially. The inhomogeneous surface layer has a thickness of about 4.9 Å. This may be compared with the value 7.6 Å determined experimentally for the thickness of the free ^{4}He surface[32] and values of around 6.0 Å found in HNC calculations carried out by other authors.[14,17] The relatively small theoretical value found here is influenced by the presence of the external potential in the Hamiltonian (1).

Numerical results on the optimized excitation energies as functions of wave number q are displayed in Fig. 3. The boundaries of the continuum regions are indicated by short-dashed lines and demonstrate the features discussed in Ref. 24. The domain of continuum states may be divided up into three distinct areas labeled L, V, and VL, corresponding in turn to the volume excitations in the bulk supported at liquid densities (L states), continuum excitations confined to the low-density regime (V states), and continuum VL states. In addition, accidental two- or threefold degeneracies may occur. The relevant taxonomy is explained in some detail in Ref. 24.

Here, our primary concern will be the bound states that can be excited in the surface layer. The calculations reveal the existence of two branches of bound states characterized by eigenvectors $|\psi_{1,q}\rangle$ and $|\psi_{2,q}\rangle$ and respective energy eigenvalues $\varepsilon_1(q)$ and $\varepsilon_2(q)$. In the energy-momentum diagram (Fig. 3), these branches extend between the domain of energetically low-lying L states and the roton region of the bulk ^{4}He liquid found at wave numbers $q\simeq q_R\simeq 1.9$ Å^{-1}. The first branch is represented by wave functions $\psi_1(z,q)$ without nodes in the surface layer and begins at zero wave number. At small wave numbers $q\leq 0.8$ Å^{-1}, the amplitudes $\psi_1(z,q)$ penetrate exponentially into the liquid domain with a characteristic penetration depth l approximately proportional to the inverse wave number. Typical examples are included in Fig. 4. These states describe surface phonons

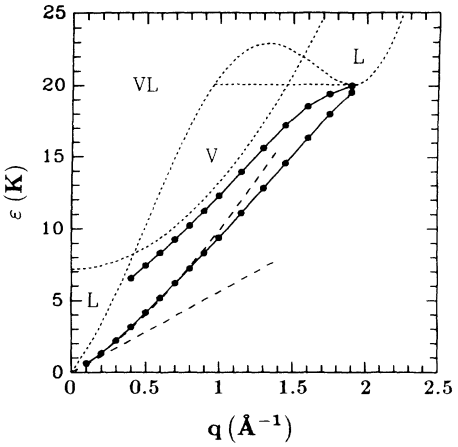

FIG. 3. Dispersion relations for elementary excitations of liquid ^{4}He with a planar surface. Excitation energies $\varepsilon(q)$ are plotted against wave number q. The boundaries of the continuous spectra of L, V, and VL states (see text and Ref. 24) are demarcated by short-dashed lines, which represent the energy $\varepsilon_L(q)$ of an elementary excitation of bulk liquid ^{4}He at density $\rho_L=0.0218$ Å^{-3} and the energy $\varepsilon_V(q)=|\mu|+\varepsilon_0(q)$ of an evaporated ^{4}He atom with momentum $\hbar\mathbf{q}$. Here $|\mu|=7.17$ K is the binding energy per particle of the bulk liquid, while $\varepsilon_0(q)=\hbar^2q^2/2m$ is the energy of a free ^{4}He atom of wave number q. There are two branches of bound surface states, with energies $\varepsilon_1(q)$ and $\varepsilon_2(q)$ ordered according to $\varepsilon_1(q)<\varepsilon_2(q)<\varepsilon_L(q)$, $\varepsilon_L(q_R)$, and $\varepsilon_V(q)$, where $q_R\simeq 1.9$ Å^{-1} is the wave number at the roton minimum of the bulk liquid. The numerical results for the dispersion relations of the bound surface modes are entered as solid dots. The solid lines interpolate these data. At wave numbers $q\leq 0.8$ Å^{-1}, the bound excitations are associated with surface phonons and capillary waves. The linear dispersion law of surface phonons is traced by the straight long-dashed line; inclusion of the dispersive contribution of capillary waves yields the upper long-dashed curve (see text, Sec. IV).

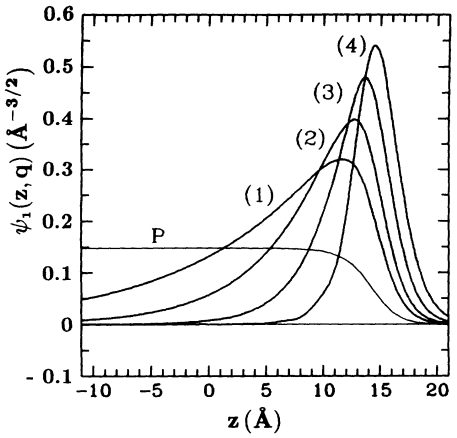

FIG. 4. Optimal wave functions $\psi_1(z,q)$ of bound excitations having no nodes in the surface region, plotted against the vertical coordinate z at small values of wave number q. Curves (1)–(4) correspond, in turn, to $q=0.1$, 0.2, 0.4, and 0.8 Å^{-1}. The curve labeled P is the square root of the density profile $\sqrt{\rho(z)}$, which represents the ground state of the Bogoliubov equation (12). Exponential penetration into the liquid is observed. These bound surface modes may be interpreted physically in terms of surface phonons and capillary waves.

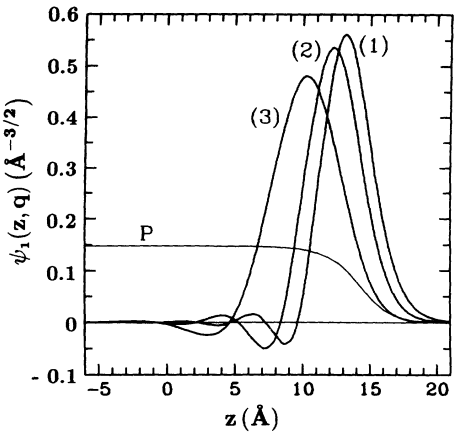

FIG. 5. Optimal wave functions $\psi_1(z,q)$ of bound excitations having no nodes in the surface region, plotted against the vertical coordinate z at large ("atomic") wave numbers q. Curves (1)–(3) correspond, in turn, to $q=1.6$, 1.75, and 1.9 Å^{-1}. The curve labeled P is the square root of the density profile $\sqrt{\rho(z)}$. These bound surface modes are interpreted as trapped rotons.

and capillary waves. As $q\to 0$, the associated excitation energies exhibit the dispersive properties known from quantized hydrodynamic treatments,[1,2] while the wave functions $\psi_1(z,q)$ smoothly approach the function $\sqrt{\rho(z)}$ that represents the ground state of the Bogoliubov equation (12). For sufficiently small wave numbers, the wave functions are therefore expected to have the asymptotic dependence[16]

$$\psi_1(z,q)\sim\sqrt{\rho(z)}e^{qz}\quad(z\to-\infty;q\to 0)\ . \tag{34}$$

At atomic wavelengths ($q\geq 1$ Å^{-1}) the excitations change their character and the wave functions are in general strongly localized in the inhomogeneous surface region centered at a local density of about $0.8\rho_L$. Figure 5 gives examples of bound-state wave functions $\psi_1(z,q)$ at three different values of the wave number q (1.6, 1.75, and 1.9 Å^{-1}). On the high-q end, the energy spectrum belonging to the first branch merges with the bulk excitation curve at a wave number close to $q_R=1.9$ Å^{-1}. Accordingly, we interpret the surface excitations in this energy-wave-number regime as rotons trapped in the surface layer. The behavior of these states and of the states of the first branch at small wave numbers will be discussed more fully in the next two sections.

In Fig. 6 we plot the wave function $\psi_2(z,q)$ at $q=0.4$ Å^{-1}. (The corresponding energy eigenvalue is $\varepsilon=6.5$ K.) This figure illustrates the typical features of the states belonging to the second branch of bound excitations, which have one node in the surface layer. At large wave numbers their energies approach the bulk roton energy $\varepsilon(q_R)$ from below. The states (or eigenvectors) $|\psi_{2,\mathbf{q}}\rangle$ have energies that are close to the continuous energy spectrum of unbound ^{4}He atoms described by V states.

IV. SURFACE PHONONS AND CAPILLARY WAVES

In this section we present a detailed analysis of the bound surface modes of the first branch, at low energies ($\varepsilon_1\leq 10$ K) and at small wave numbers ($q\leq 1$ Å^{-1}). Our discussion of the propagation of these waves is framed in terms of a specialized version of the Bogoliubov equation (12). We first extract the optimal excitation energy $\varepsilon_1(q)$ of the branch of states $|\psi_{1,\mathbf{q}}\rangle$ as a function of wave number q. For economy of notation the subscripts 1 and $\mathbf{q}$ will be dropped; thus $|\psi\rangle$, $\psi(z,q)$, and $\varepsilon(q)$ denote a bound state of the lowest branch, its wave function, and its energy, respectively.

The proposed specialization has been formulated in Ref. 21 so as to yield a useful stability condition on the

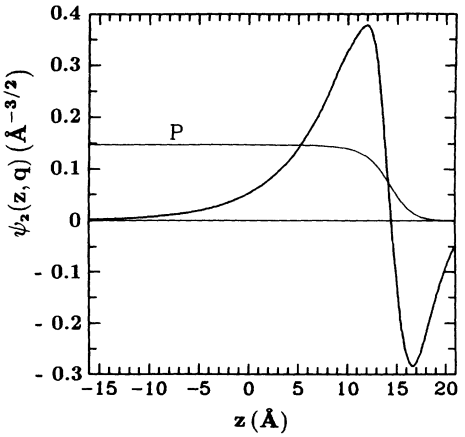

FIG. 6. Optimal wave function $\psi_2(z,q)$ of a bound excitation having one node in the inhomogeneous surface layer, plotted against the vertical coordinate z for the wave number $q=0.4$ Å^{-1}. This wave function represents a surface state of energy $\varepsilon_2=6.5$ K that belongs to the second branch of bound states. The curve labeled P is the square root of the density profile, $\sqrt{\rho(z)}$.

elementary excitations [see Eq. (3.8) therein]. For present purposes it is convenient to cast the dispersion relation into the form

$$\varepsilon^2(q)=q^{-1}\varepsilon_0(q)F(q)D(q) \tag{35}$$

with a driving potential

$$D(q)=\varepsilon^{\dagger}(q)+2V_S^{\dagger}(q)\ . \tag{36}$$

The energy components $\varepsilon^{\dagger}(q)$ and $V_S^{\dagger}(q)$ at given wave number q are defined by the expectation values

$$\varepsilon^{\dagger}(q)=\frac{\langle\psi|(H_0+\varepsilon_0)^3|\psi\rangle}{\langle\psi|(H_0+\varepsilon_0)^2|\psi\rangle} \tag{37}$$

and

$$V_S^{\dagger}(q)=\frac{\langle\psi|(H_0+\varepsilon_0)\hat{V}(q)(H_0+\varepsilon_0)|\psi\rangle}{\langle\psi|(H_0+\varepsilon_0)^2|\psi\rangle} \tag{38}$$

with $\varepsilon_0=\varepsilon_0(q)=\hbar^2q^2/2m$, the operator H_0 being defined by Eq. (11). The particle-hole potential operator $\hat{V}(q)$ at given wave number q is defined by the coordinate space matrix elements $\sqrt{\rho(z_1)\rho(z_2)}V_{\rm ph}(q,z_1,z_2)$, where $V_{\rm ph}(q,z_1,z_2)$ is the Hankel transform of the particle-hole potential $V_{\rm ph}(\eta,z_1,z_2)$.

The dispersion relation (35) furthermore involves a penetration factor

$$F(q)=\frac{q\langle\psi|(H_0+\varepsilon_0)^2|\psi\rangle}{\varepsilon_0\langle\psi|H_0+\varepsilon_0|\psi\rangle}\ . \tag{39}$$

The function $F(q)$ and the energy $\varepsilon^{\dagger}(q)$ are positive quantities by construction. The energy expression (35) with the driving potential (36) is the analog of the familiar dispersion relation[11,12]

$$\varepsilon^2(q)=\varepsilon_0(q)[\varepsilon_0(q)+2V_L(q)] \tag{40}$$

of the elementary excitations in bulk liquid ^{4}He described by plane waves. In the latter case, the quantity $V_L(q)$ is the dimensionless three-dimensional Fourier transform of the isotropic particle-hole potential at density ρ_L, and the penetration factor $F(q)$ reduces to $F(q)=q$. The speed c of ordinary sound waves follows directly from expression (40) by taking the limit $q\to 0$ to obtain

$$mc^2=V_L(0)\ . \tag{41}$$

To check the accuracy of our numerical techniques for dealing with the inhomogeneous system, we employ the results on the potential $V_{\rm ph}(\eta,z_1,z_2)$ deep inside the liquid (i.e., at large negative values of z_1 and z_2) to calculate the corresponding speed of sound via Eq. (41). The result is $mc^2=20.14$ K or $c=204.51$ m/sec. This is in fair agreement with the result $mc^2=18.67$ K or $c=197.34$ m/sec determined for homogeneous liquid ^{4}He within the analogous variational ansatz for the homogeneous fluid.

The numerical findings on quantities (36)–(39) are summarized in Figs. 7–11. The penetration factor (Fig. 7) has a finite nonzero value $F(0)$ at $q=0$ and displays an initially linear increase with wave number q. At $q\simeq 1$ Å^{-1} the curve $F(q)$ has an inflection point and, near the roton wave number $q_R=1.9$ Å^{-1}, closely approaches the penetration factor $F_L(q)=q$ that characterizes the homogeneous bulk liquid. Figure 8 shows the numerical results for the energy $\varepsilon^{\dagger}(q)$ of Eq. (37) in the whole range of wave numbers q at which surface states exist. This energy is nonzero at $q=0$ and depends quadratically on wave number in the range $q\le 0.8$ Å^{-1}. We may check the numerical calculation of $\varepsilon^{\dagger}(q)$ at zero wave number by comparing with the analytic result for $\varepsilon^{\dagger}(0)$ implied by the asymptotic formula (34). Insertion of Eq. (34) into Eq. (37) yields

$$\varepsilon^{\dagger}(0)=\frac{\hbar^2}{2m}\int_{-\infty}^{\infty}[\rho(\partial^2\ln\rho)^2](z)dz\Big/\int_{-\infty}^{\infty}[\rho(\partial\ln\rho)^2](z)dz. \tag{42}$$

Using the numerical results on the density profile $\rho(z)$ as input data, we may calculate the integrals and arrive at the value $\varepsilon^{\dagger}(0)\simeq 1.4$ K. This value is in good accord with the data on $\varepsilon^{\dagger}(q)$ plotted in Fig. 8.

The numerical results for the optimal particle-hole energy (38) of bound surface states at wave numbers $q\le 1$ Å^{-1} are presented in Fig. 9. The data for the quantity $V_S^{\dagger}(q)$ (calculated at $q=0.1$ Å^{-1},0.2 Å^{-1},...) are linearly extrapolated to zero wave number and matched to the condition

$$D(0)=\varepsilon^{\dagger}(0)+2V_S^{\dagger}(0)=0\ . \tag{43}$$

This condition is required by classical fluid dynamics if gravitational waves are absent. We could, of course, incorporate the effect of waves due to external gravitational forces by supplementing the potential (2) with an additive term $-g_Sz$, where g_S is the gravitational acceleration at the earth's surface.

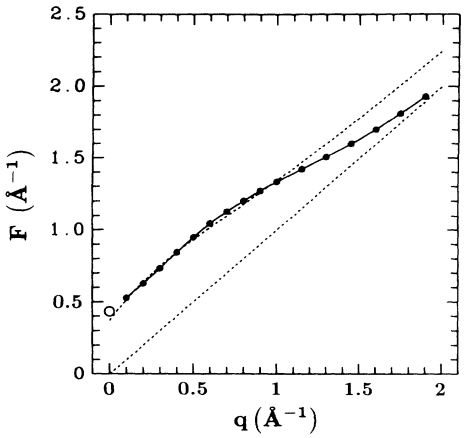

FIG. 7. Penetration factor $F(q)$ of Eq. (39) as a function of wave number q. The numerical results from the optimization procedure (dots) are suitably interpolated (solid curve) and extrapolate toward the appropriate value at wave number $q=0$ (open circle). The trend of the data indicates that at high q the function $F(q)$ merges into the bulk penetration factor q of rotons (lower short-dashed line). The upper short-dashed line shows the approximation for $F(q)$ based on the analytic ansatz (50), applicable for low wave numbers ($0\le q\le 0.8$ Å^{-1}).

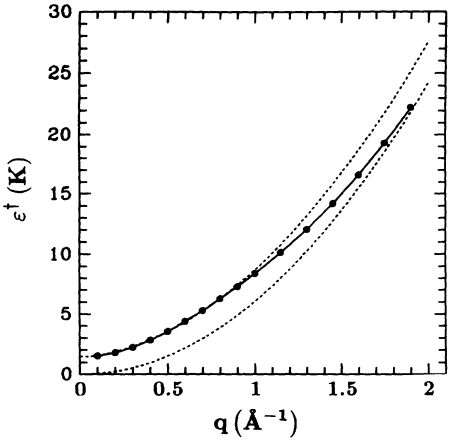

FIG. 8. Expectation value $\varepsilon^{\dagger}(q)$ of Eq. (37), plotted as a function of wave number q. This quantity contributes to the driving potential (36) of energy relation (35). The numerical results from the optimization procedure are represented by dots and are suitably interpolated by the solid curve. As $q \to 0$ the solid curve behaves quadratically, taking a nonzero positive value at zero wave number [cf. Eq. (42)]. In the roton region of large momenta, it approaches the kinetic energy $\varepsilon_0(q)=\hbar^2 q^2/2m$ of a free ^{4}He atom. The lower short-dashed curve is the parabola $\varepsilon_0(q)$. The analytical result for $\varepsilon^{\dagger}(q)$ based on the ansatz (50) yields the upper short-dashed curve.

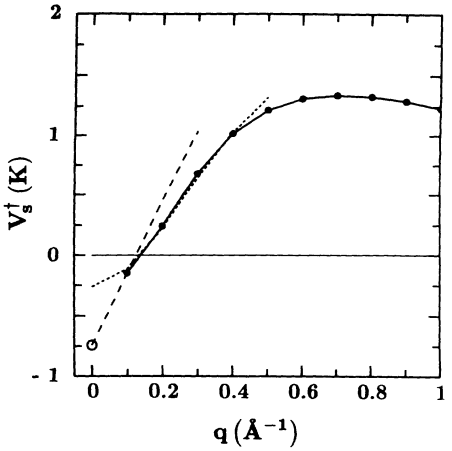

FIG. 9. Particle-hole energy $V_S^{\dagger}(q)$ [Eq. (38)] of bound surface states without nodes in the surface region, plotted against wave number q in the long-wavelength regime. Numerical data from the optimization procedure are shown as dots and are suitably interpolated to yield the solid curve. The open circle marks the value $V_S^{\dagger}(0)$ derived from condition (43). This circle is joined to the first data point by a straight long-dashed line, the slope of which coincides with the slope of the driving potential $D(q)$ (see Fig. 10). The approximate result for $V_S^{\dagger}(q)$ corresponding to the simple analytic ansatz (50) is included as the short-dashed curve.

The driving potential $D(q)$ defined by Eq. (36) depends linearly on q at sufficiently small q values. This behavior is indeed clearly demonstrated by our numerical results on the energy factor $D(q)$, as may be seen in Fig. 10. Strong deviations from linearity appear at wave numbers $q \gtrsim 0.5$ Å^{-1}.

To make contact with the quantized hydrodynamic theory,[1,2] it is assumed that the penetration factor (39) and the driving potential (36) may be expanded in powers of the wave number q. In accordance with our numerical results and condition (43), we thus assert

$$F(q)=F(0)+\dot{F}(0)q+\cdots , \tag{44}$$

$$D(q)=\dot{D}(0)q+\tfrac{1}{2}\ddot{D}(0)q^2+\cdots . \tag{45}$$

Substitution of these series into the dispersion relation (35) generates the expansion

$$\varepsilon^2(q)=\frac{\hbar^2}{m}\left[mc_S^2 q^2+\frac{\sigma}{\rho_L}q^3+\cdots\right] \tag{46}$$

for the excitation energy of the lowest bound state of wave number q, with the coefficients

$$2mc_S^2=F(0)\dot{D}(0) , \tag{47}$$

and

$$\sigma=\frac{\rho_L}{2}[\dot{F}(0)\dot{D}(0)+\tfrac{1}{2}F(0)\ddot{D}(0)] . \tag{48}$$

The first term in expression (46) is attributed to surface phonons or surface sound, while the second is associated with capillary waves driven by the surface tension. The result (47) permits evaluation of the speed of surface sound c_S in terms of the penetration factor $F(0)$ and the driving factor $\dot{D}(0)$, which is generated by the external potential and takes account also of correlation effects due to the strong internal forces. This relation is the analog of Eq. (41) describing ordinary bulk sound. More importantly, it replaces the phenomenological formula[1,2]

$$mc_S^2=df , \tag{49}$$

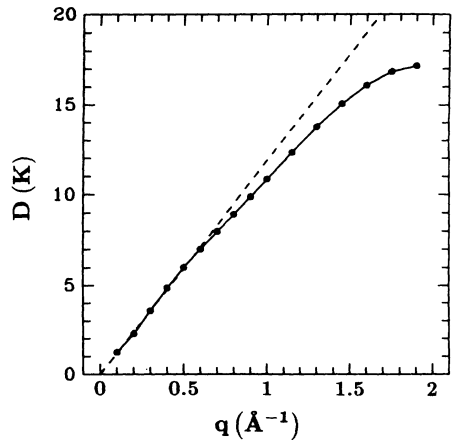

FIG. 10. Driving potential $D(q)$ of Eq. (36) as a function of wave number q. The solid dots are the numerical results from the optimization procedure, and the solid line interpolates these data. The function $D(q)$ vanishes linearly as $q \to 0$ (dashed straight line). Its slope $\dot{D}(0)$ at wave number $q=0$ determines the velocity of surface phonons. The numerical prediction for $D(q)$ levels off around the bulk roton wave number $q_R \simeq 1.9$ Å^{-1}.

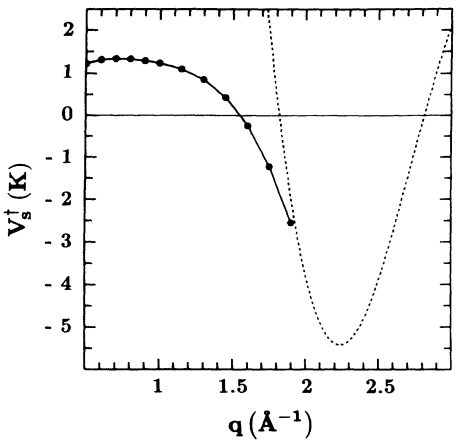

FIG. 11. Particle-hole energy $V_S^\dagger(q)$ [Eq. (38)] of bound surface states without nodes in the surface layer, plotted against wave number q at atomic wavelengths (and hence referring to trapped rotons). The solid curve interpolates the numerical data from the optimization procedure, which appear as solid dots. In the roton region corresponding to wave numbers $q \simeq q_R = 1.9$ Å^{-1}, the solid curve approaches the analogous particle-hole energy $V_L(q)$ of bulk excitations (traced by the short-dashed curve).

involving the film or surface thickness d and the strength f of the external force, by an *ab initio* dispersion rule derived from CBF theory.

Similarly, the result (48) provides a microscopic prescription for calculating the quantity σ that controls the phase velocity of capillary waves. In the absence of an external potential, $U_{\rm ext} \equiv 0$, and assuming that the system is incompressible, the coefficient σ may be identified with the surface tension.[2]

Using the actual values $F(0) = 0.433$ Å^{-1}, $\dot{F}(0) = 0.92$, $\dot{D}(0) = 11.9$ K Å, and $\ddot{D}(0) \approx 0$ determined by extrapolating our numerical results for the penetration factor $F(q)$ and for the driving potential $D(q)$ to $q = 0$, we arrive at the value $mc_S^2 = 2.6$ K or $c_S = 73$ m/sec for the speed of surface sound and the value $\sigma = 0.12$ K Å^{-2} for the coefficient (48). The excitation energies of the lowest-lying surface modes, as given by numerical solution of Eq. (12), essentially follow the hydrodynamic dispersion law (46) in the range of wave numbers $q \leq 0.8$ Å^{-1}. This can be clearly seen by comparing the numerical results for the excitation energy $\varepsilon_1(q)$ with results from expansion (46), which are represented in Fig. 3 by the lower long-dashed line (surface sound only) and the upper long-dashed line [surface sound modified by the cubic term in Eq. (46)].

Finally, we point out that the various quantities (36)–(39) at wave numbers $q \leq 0.6$ Å^{-1} may be well reproduced by assuming the simple analytic expression

$$\psi(z,q) \simeq \sqrt{\rho(z)}\, e^{qz}(1 + a_0 e^{qz})^{-1} \tag{50}$$

as an approximate representation of the optimal wave function $\psi(z,q)$ calculated within variational-CBF theory. The ansatz (50) is, of course, in agreement with the asymptotic property (34). The numerical data are best fitted by adopting a parameter value $a_0 = 0.2$, if we choose the origin $z = 0$ to be at the Gibbs surface. Insertion of Eq. (50) into the expectation values (37)–(39) and evaluation of the corresponding integrals leads us to approximate results for the functions $F(q)$, $\varepsilon^\dagger(q)$, $V_S^\dagger(q)$, and $D(q)$ which are indicated in Figs. 7–10. These approximations match the numerical results of the variational-CBF approach quite well for wave numbers $q \leq 0.6$ Å^{-1}.

V. TRAPPED ROTONS

We now turn to a detailed analysis of our numerical results for the optimal bound states and their energies at large wave numbers ($q > 1$ Å^{-1}). We proceed in the same manner as in the preceding section, examining the wave functions and explicating the dispersion law (35).

For large q the wave functions $\psi(z,q)$ of the bound surface modes of the first branch are centered at relatively high local density on the liquid side of the Gibbs surface (see Fig. 5). For this class of states, the influence of the energy operator H_0 on the expectation values (37)–(39) should become very small at such densities and wave numbers. Neglecting the effects of H_0 in Eqs. (37)–(39), we are led to the approximations $F(q) \approx q$ and $\varepsilon^\dagger(q) \approx \varepsilon_0(q)$. The particle-hole quantity $V_S^\dagger(q)$ for the bound surface states, given by Eq. (38), then reduces to the approximate form

$$V_S^\dagger(q) \approx V_S(q) = \frac{\langle \psi | \hat{V}(q) | \psi \rangle}{\langle \psi | \psi \rangle} \ . \tag{51}$$

The dispersion relation of bound surface modes with large wave numbers, $q \approx q_R$, may therefore be given the approximate expression

$$\varepsilon^2(q) \approx \varepsilon_0(q)[\varepsilon_0(q) + 2V_S(q)] \ . \tag{52}$$

The result (52) should be compared with the energy-momentum relation (40) for bulk excitations in liquid ^{4}He. Patently, relations (52) and (40) differ only in the potential portion. Equation (52) involves the surface particle-hole energy $V_S(q)$ instead of the analogous bulk quantity $V_L(q)$. Since the states $|\psi\rangle$ are localized at a density ρ rather close to the bulk density ρ_L, the surface potential operator $\hat{V}(q) = \tilde{V}_{\rm ph}(q, z_1, z_2)$ should not differ much from the corresponding quantity $\rho_L V_{\rm ph}(q, |z_1 - z_2|)$ generated from the bulk particle-hole potential $V_{\rm ph}(|\mathbf{r}_1 - \mathbf{r}_2|)$. Accordingly, the difference $V_L(q) - V_S(q)$ should be quite small in the range of q around the roton wave number q_R where the bound surface state branch approaches the liquid domain of the continuous spectrum.

The properties educed above are confirmed by the numerical results on the optimal functions $F(q)$ and $\varepsilon^\dagger(q)$ for $q \approx q_R$. These data are plotted in Figs. 7 and 8. We see from Fig. 7 that the penetration factor $F(q)$ does indeed closely approach the straight line q that represents the bulk penetration factor as $q \to q_R$. The analogous feature of the quantity $\varepsilon^\dagger(q)$ is seen in Fig. 8. At q near q_R our numerical results for $\varepsilon^\dagger(q)$ are very close to the kinetic energy $\varepsilon_0(q) = \hbar^2 q^2/2m$ of a free ^{4}He atom.

It is particularly illuminating to compare the numeri-

cal results for the optimal particle-hole energies $V_S^{\dagger}(q)$ and $V_L(q)$ in the region of the roton wave number q_R (see Fig. 11). The surface quantity $V_S^{\dagger}(q)$ reaches a maximum at $q \approx 0.7$ Å^{-1} (see also Fig. 9) and thereafter decreases with increasing wave number, approaching the very steep potential $V_L(q)$ close to q_R. The latter behavior is indicative of a level-crossing phenomenon around the bulk roton minimum. The similarity between the dispersion relations (40) and (52) on the one hand, and the nature of the results for the driving forces $V_S^{\dagger}(q)$ and $V_L(q)$ on the other, point to an intimate relation between rotons and the surface modes at large momenta. Bulk rotons at $q \approx q_R$ respond to the strength $V_L(q)$, while the surface modes at atomic wavelengths are driven by the corresponding surface quantity $V_S(q)$. We therefore interpret these surface modes at large energies as rotons trapped in the surface layer.

Figure 10 displays the driving term $D(q)$ over the range of accessible wave numbers. This function begins to deviate from the linear behavior characteristic of small wave numbers at about $q \simeq 0.5$ Å^{-1} and becomes essentially constant at large q values around the wave number q_R of a roton. Using these properties it would be straightforward to construct a simplified dispersion law for the trapped rotons that effectively approximates the corresponding numerical results on the first-branch excitation energies, as generated by the variational-CBF approach and sketched in Fig. 3.

VI. CONCLUDING REMARKS

This paper has continued and expanded upon the investigation of the vapor-liquid ^{4}He interface that was begun in Ref. 24. Specifically, we have devised and implemented an appropriate and efficient computational procedure for *ab initio* analysis of the bound surface states and their energies, at zero temperature. The treatment employs the variational-CBF approach to calculate the optimal density profile $\rho(z)$ and the optimal non-nodal elements $X(q,z_1,z_2)$ that characterize the spatial distribution function $g(\mathbf{r}_1,\mathbf{r}_2)$, while determining the optimal Feynman excited states and excitation energies. Results of this *ab initio* theory for the bound states and their dispersive properties have been obtained over the full range of wave numbers $0 \leq q \leq q_R$ at which these surface excitations can be generated. We have given an explicit microscopic description of the optimal excitation energies at small wave numbers by evaluating the speed of surface sound and the phase velocity of capillary waves. The attendant analysis and computation improve upon the familiar quantized hydrodynamic description[1,2] of surface phonons and waves driven by surface tension. Further, the present variational-CBF treatment facilitates a systematic theoretical discussion of the surface excitations at atomic wavelengths. However, since we ignore backflow effects, the numerical results for the wave functions and energies of trapped rotons must still be regarded as semiquantitative. The incorporation of backflow is tractable within the CBF formalism and should be attempted in future work. Based on this more sophisticated treatment, it would be important to pursue a CBF study of the ^{4}He surface when external forces are absent, i.e., the free helium surface.

However, we believe that in the near term it would be more fruitful to exploit the formalism and the numerical techniques developed here in a variety of interesting problems that conform to the existing framework. For example, one could vary the strength U_0 or replace the external potential (2) by realistic adhesive potentials or van der Waals forces and examine in detail their influence on the energy spectrum, and, notably, on the phase velocity of surface sound and capillary waves. This project would be especially timely in light of recent measurements on third sound.[33]

In fact, a first step in this direction has already been taken. Calculations have been performed over quite wide ranges of the strength and width parameters of the potential (2), without seeing drastic changes of the excitation spectrum on the scale of Fig. 3. Such manipulations of the external potential primarily affect the values of the quantities c_S and σ in the dispersion relation (46). The number of surface excitation branches depends mainly on the surface thickness and thus indirectly on the strength and width of the external potential. Over fairly broad ranges in these potential parameters and in the surface thickness, two branches of surface modes appear in the spectrum. This is the same number of branches as found in studies of symmetric ^{4}He films in Refs. 14, 21, 22, and 31. A comparison with the findings of Ref. 24 is useful, although there the density profile and two-body correlations were not calculated within CBF theory (as has been done here); instead, phenomenological forms for these quantities were employed. The very thick surface profile of Ref. 24 evidently leads to a larger number of branches of surface modes. The calculations of this earlier work were carried out without an external potential, which is not needed if one is content with phenomenological one- and two-body correlations.

A more challenging goal is to extend the variational-CBF optimization to interfacial modes at nonzero temperature. This effort may begin with further formal development of the correlated density-matrix theory,[34,35] which would entail certain advances necessary for a proper account of the effects generated by temperature and density variations. Other interesting possibilities include the use of variational-CBF theory to study the influence of a two-dimensional lattice of electrons on the liquid ^{4}He surface and on the excitation of bound surface states,[29] and to gain a quantitative microscopic understanding of Andreev states.[28]

Concluding this discussion of future prospects, we point out that the methods we have explored may be adapted to the treatment of elementary excitations in other quantum many-body systems of quite different nature, such as popular lattice gauge models of field theories[36] or correlated spin models of interest in condensed-matter physics.[37,38]

ACKNOWLEDGMENTS

This work was supported, in part, by the Division of Materials Research and the Physics Division of the U.S. National Science Foundation under Grants No. PHY90-

02863 and PHY93-07484 and by the Deutsche Forschungsgemeinschaft under Grant No. Ri267/20-1. K. A. Gernoth gratefully acknowledges financial support from the BASF Aktiengesellschaft and the Studienstiftung des deutschen Volkes. We thank K. E. Kürten and L. Szybisz for advice during the design of the numerical optimization procedures. We have also benefited from an informative discussion with E. Krotscheck.

[1]K. R. Atkins, Can. J. Phys. **31**, 1165 (1953); Phys. Rev. **113**, 962 (1959).
[2]D. O. Edwards and W. F. Saam, in *Progress in Low Temperature Physics,* edited by D. F. Brewer (North-Holland, Amsterdam, 1978), Vol. 7A.
[3]P. J. King and A. F. G. Wyatt, Proc. R. Soc. London, Ser. A **322**, 355 (1971).
[4]K. A. Pickar and K. R. Atkins, Phys. Rev. **178**, 399 (1969).
[5]H. J. Lauter, H. Godfrin, and P. Leiderer, J. Low Temp. Phys. **87**, 425 (1992).
[6]H. J. Lauter, H. Godfrin, V. L. P. Frank, and P. Leiderer, Phys. Rev. Lett. **68**, 2484 (1992).
[7]C. C. Chang and M. Cohen, Phys. Rev. B **11**, 1059 (1975).
[8]G. Ji and M. Wortis, Phys. Rev. B **34**, 7704 (1986).
[9]L. Pitaevskii and S. Stringari, Phys. Rev. B **45**, 13 133 (1992).
[10]J. W. Clark and E. Feenberg, Phys. Rev. **113**, 388 (1959).
[11]E. Feenberg, *Theory of Quantum Fluids* (Academic, New York, 1969).
[12]C. W. Woo, in *The Physics of Liquid and Solid Helium,* edited by K. H. Bennemann and J. B. Ketterson (Wiley, New York, 1976).
[13]C. E. Campbell, in *Progress in Liquid Physics,* edited by C. A. Croxton (Wiley, New York, 1978).
[14]E. Krotscheck, G.-X. Qian, and W. Kohn, Phys. Rev. B **31**, 4245 (1985).
[15]E. Krotscheck, Phys. Rev. B **31**, 4258 (1985); **32**, 5713 (1985); **33**, 3158 (1985).
[16]E. Krotscheck, S. Stringari, and J. Treiner, Phys. Rev. B **35**, 4754 (1987).
[17]M. Saarela, P. Pietiläinen, and A. Kallio, Phys. Rev. B **27**, 231 (1983).
[18]R. P. Feynman, Phys. Rev. **94**, 262 (1954).
[19]R. P. Feynman and M. Cohen, Phys. Rev. **102**, 1189 (1956).
[20]J. L. Epstein and E. Krotscheck, Phys. Rev. B **37**, 1666 (1988).
[21]L. Szybisz and M. L. Ristig, Phys. Rev. B **40**, 4391 (1989).
[22]L. Szybisz, Phys. Rev. B **41**, 11 282 (1990).
[23]E. Krotscheck and C. J. Tymczak, Phys. Rev. B **45**, 217 (1992).
[24]K. A. Gernoth and M. L. Ristig, Phys. Rev. B **45**, 2969 (1992).
[25]J. W. Clark, in *Progress in Particle and Nuclear Physics,* edited by D. Wilkinson (Pergamon, New York, 1979), Vol. 2.
[26]T. Morita and K. Hiroike, Prog. Theor. Phys. **25**, 537 (1961).
[27]J. Mathews and R. L. Walker, *Mathematical Methods in Physics* (Benjamin, New York, 1970).
[28]A. F. Andreev, Zh. Eksp. Teor. Fiz. **50**, 1415 (1966) [Sov. Phys. JETP **23**, 939 (1966)].
[29]P. Leiderer, J. Low. Temp. Phys. **87**, 247 (1992).
[30]S. Stringari and J. Treiner, Phys. Rev. B **36**, 8369 (1987).
[31]L. Szybisz and R. O. Vallejos, in *Condensed Matter Theories,* edited by A. N. Proto and J. L. Aliago (Plenum, New York, 1992), Vol. 7.
[32]L. B. Lurio, T. A. Rabedau, P. S. Pershan, I. F. Silvera, M. Deutsch, S. D. Kosowsky, and B. M. Ocko, Phys. Rev. B **48**, 9644 (1993).
[33]J. G. Brisson, J. C. Mester, and I. F. Silvera, Phys. Rev. B **44**, 12 453 (1991).
[34]G. Senger, M. L. Ristig, K. E. Kürten, and C. E. Campbell, Phys. Rev. B **33**, 7562 (1986).
[35]G. Senger, M. L. Ristig, C. E. Campbell, and J. W. Clark, Ann. Phys. (N.Y.) **218**, 160 (1992).
[36]A. Dabringhaus, M. L. Ristig, and J. W. Clark, Phys. Rev. D **43**, 1978 (1991).
[37]M. L. Ristig, Z. Phys. B **79**, 351 (1990).
[38]F. Kusmartsev and M. L. Ristig, Phys. Rev. B **44**, 5351 (1991).